Assessment of Land Cover Changes in the Allala Watershed Based on Object Based Image Analysis Using Landsat and Sentinel-2 Images

Narimane Zaabar, Simona Niculescu, and Mustapha Kamel Mihoubi

Abstract The coastal city of Ténès, located in northwestern Algeria, is exposed to several natural hazards, such as floods, earthquakes, landslides, and forest fires. Due to human activities, socio-economic constructions, agricultural activities, and the resulting population acceleration, land cover and land use (LULC) dynamics in the city are changing over time. Hence, the understanding of LULC changes and its interactions with human activities and natural hazards is essential for appropriate land management and decision-making. In this study, we investigate LULC changes in the Allala watershed, including the city of Ténès, using remote sensing methods and Geographic Information System (GIS) tools. Object-based image analysis (OBIA) based on random forest (RF) and support vector machine (SVM) machine learning algorithms was performed to provide LULC classification maps, and then, LULC changes were assessed using GIS. In order to assess LULC changes, we used three images acquired using remote sensing, corresponding to 3 years; 1999, 2009, and 2020. A Sentinel-2 image and two Landsat images were used as input data in our methodology. Our LULC classification results showed that RF outperformed SVM on the three input data periods, with an overall accuracy of 95.6% obtained with the Sentinel-2 image. Given the changes over time, it is clear that the Allala watershed has undergone significant changes over the years, particularly an increase

N. Zaabar (✉)
University of Western Brittany, CNRS, LETG Brest UMR 6554 CNRS, Technopôle Brest-Iroise, Plouzané-Brest, France

ENSH, National Higher School of Hydraulics, MVRE, Laboratoire de Mobilisation et valorisation des ressources en eau, Blida, Algeria

S. Niculescu
Laboratory LETG-Brest, UMR 6554 CNRS, University of Western Brittany, Plouzané, France
e-mail: simona.niculescu@univ-brest.fr

M. K. Mihoubi
ENSH, National Higher School of Hydraulics, MVRE, Laboratoire de Mobilisation et valorisation des ressources en eau, Blida, Algeria
e-mail: n.zaabar@ensh.dz

S. Niculescu (ed.), *European Spatial Data for Coastal and Marine Remote Sensing*, https://doi.org/10.1007/978-3-031-16213-8_5

in building infrastructure and agricultural land due to population and urbanization growth. Analyzing and mapping the trends of LULC changes in the study area provide a basis for strategic planning and managing, and results of LULC changes can be used as a decision support tool and provide further help in regional and national land management.

Keywords LULC changes · Allala watershed · Landsat images · Sentinel-2 · Object-based image analysis (OBIA) · RF · SVM

1 Introduction

Land use and land cover (LULC) is considered a critical environmental issue with global implications in environmental management and sustainable development [16, 32]. In fact, due to natural and artificial factors, LULC around the world is still undergoing considerable changes, most notably changes due to climate change, rapid urbanization (mainly in critical areas), population growth that requires urban agglomeration development, and the subsequent construction land expansion.

The coastal town of Ténès, located in northwestern Algeria, has observed an increase in changes in LULC due to diverse causes. Indeed, the region is exposed to ongoing natural disasters, such as earthquakes and landslides [2, 29], and natural hazards such as landscape degradation and flash floods [22] due to climate changes, which highly modify LULC dynamics because of the hydrological process of flash floods [13, 14]. At the same time, the region experiences significant deforestation and many forest fires, such as the one in 2014 [7]. As a part of a sustainable development strategy and because of its privileged location, both historical and touristic, the city has integrated several projects based on human activities, socio-economic constructions, and agricultural activities. This implicates population growth and urban construction, as well as the evolution of agricultural areas and, in consequence, population acceleration, as factors that directly lead to changes in the LULC trends of the city over time. In this context, rapid data acquisition and detection of LULC changes are an essential element in environmental monitoring, urban planning, and sustainable development. Additionally, the understanding of LULC dynamics and changes, and its interactions with human activities and natural hazards, is essential for appropriate land management and decision-making improvements [37]. Furthermore, LULC changes and evolution information is considered critical for several environmental considerations, such as water resource management and natural hazard assessment [6, 27, 36, 40].

In recent decades, remote sensing has become more widespread in the scientific field and has emerged as a useful way to track LULC changes based on LULC classification techniques [10, 18, 24]. Pixel-based image analysis methods have been the most widely used to produce LULC maps [25, 30]. These methods consider only the spectral characteristics of the input image, which implies certain limitations of the produced classifications of LULC and any trend detection. These limitations

may be partially overcome by considering other image features in order to detect LULC classes with high accuracy [8, 9].

Consequently, the use of object-based image analysis (OBIA) and machine learning classifiers has emerged in the remote sensing community as a way to better address LULC classification and change detection. This method considers the spectral, textual, and contextual information of pixels. Recently, OBIA classification has now replaced conventional pixel-based methods and will facilitate land cover classification using high spatial resolution remote sensing imagery [8, 17, 38]. In addition, according to previous studies, this method has successfully provided the accurate classification of LULC changes using high- and very-high-resolution images [1]. provided LULC maps using Landsat images for 1985, 1990, 2000, 2007, and 2014 for five cities of Saudi Arabia. The aim of their study was to assess the urban growth in these cities. LULC classification was carried out using an OBIA approach. The classified images were also used to predict LULC changes and the growth of urban areas for 2024 and 2034 using specific models. Changes were assessed through transition probabilities. Extreme Gradient Boosting (XGBoost)-based informative feature selection and the random forest algorithm were used to ensure the OBIA classification. The results of LULC classification showed higher values of the overall accuracy (OA), up to 90%, which was very beneficial in assessing LULC [20]. applied the OBIA method in order to classify LULC and evaluate the changes in the Cameron Highlands in Malaysia by taking advantage of the OBIA considerations of texture, shape, position, and digital number, as well as a series of band combinations. As remote sensing data, the authors used Landsat time series images from 2009 to 2019. Similarly, [28] mapped LULC changes in the core zone sand dune located in Indonesia using aerial images taken between 2015 and 2020. The nearest neighbor algorithm was used for LULC classification after a segmentation process. Analysis of the land use changes was carried out by comparing the land use classification results of 2015 and 2020.

The aim of this study is the assessment of the spatio-temporal patterns of LULC across the Allala watershed over a 21-year period (1999–2020), based on remote sensing methods and GIS applications. First, OBIA classification–based machine learning algorithms (random forest and support vector machine) were employed to map LULC over 3 years: 1999, 2009, and 2020. Then, based on the more accurate LULC maps, the assessment of LULC changes was conducted using post classification analysis implemented using GIS applications.

2 Study Area

The study area is the Oued Allala watershed located in northern Algeria on the Mediterranean coast. The watershed covers a total area of 307 km^2 with a length of 35 km for its principal thalweg (Fig. 1). The area is situated between the maximum and minimum altitude, 989 m and 0 m, respectively, and includes Ténès City, a tourist and port city and the second largest city in the Chlef Wilaya. The region is

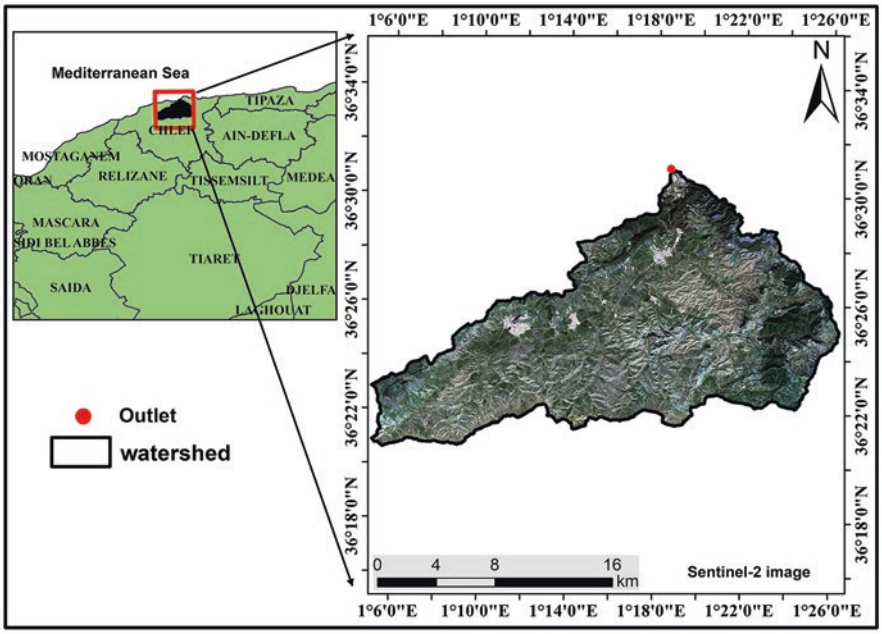

Fig. 1 Location of the study area

influenced by the Mediterranean climate and is characterized by a warm and temperate climate with significant precipitation in the winter months [39]. The average temperature is 18.6 °C and the average total annual rainfall is around 585 mm [22]. The Oued Allala watershed is an area with a high degree of landscape diversity, including the presence of human settlements, forests, and agricultural areas. The northern parts of the Allala catchment are covered by pine forest. Annual crops such as cereals cover the southern part of the watershed. This diversity in LULC classes necessitates an accurate classification and the monitoring of LULC changes.

In addition, as a part of the national strategy to combat natural hazards, specifically floods, the Ténès region was chosen for this study because of its regional importance, its geographical location, and its elevated risk of natural hazards, mainly floods. The analysis of LULC in this area is critical input information for flood vulnerability assessment.

3 Material and Methods

Through a consecutive process, we mapped and assessed land cover/use changes in the Allala watershed for over 21 years. Remote sensing methods combined with GIS applications were both used. Both Landsat and Sentinel-2 data were acquired to establish the classification following two essential steps: (1) The object-based

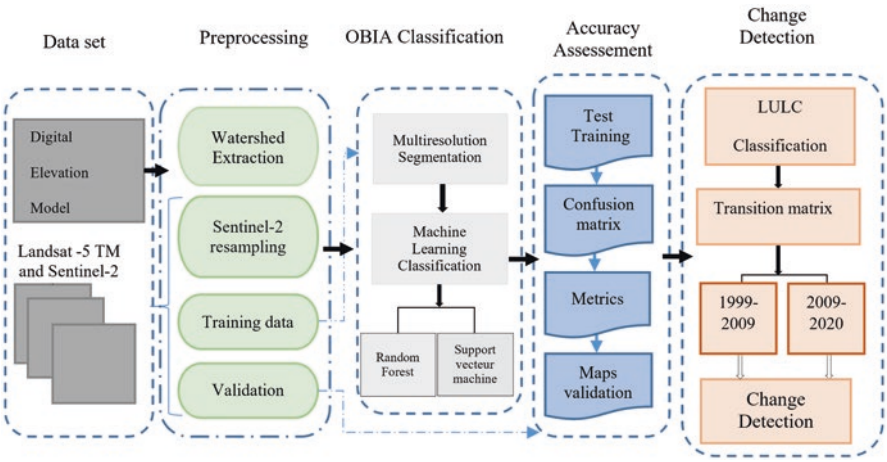

Fig. 2 Workflow of the proposed methodology

image analysis (OBIA) method was applied to provide land cover/use maps with two machine learning algorithms, random forest (RF) and support vector machine (SVM). (2) Then, the assessment of LULC changes was conducted in ArcMap software (version 10.8.1) by post-classification analysis and transition matrix generation (Fig. 2).

3.1 Object-Based Image Analysis (OBIA)

3.1.1 Data Acquisition and Preprocessing

Two different types of remote sensing images were acquired from the Landsat and Sentinel-2 sensors to detect LULC changes and facilitate classification. The two Landsat-5 Thematic Mapper (TM) images, with 30 m of resolution, were acquired on April 10, 1999, and May 8, 2009. Landsat-5 TM data are available with free access from the USGS Global Visualization Viewer (https://glovis.usgs.gov). The Landsat-5 TM images were already corrected.

The third image used is a Sentinel-2 image acquired on March 8, 2020, with atmospheric correction. Sentinel-2A contains 13 spectral bands, including four bands with 10 m spatial resolution, six bands with 20 m spatial resolution, and three bands with 60 m spatial resolution. A resampling into a spatial resolution of 10 m was applied in the Sentinel platform (SNAP) software before using the image in the classification process [37]. The dates were selected based on image quality (absence of cloud cover), availability, and the same season for the 3 years (1999, 2009, and 2020), in order to better detect LULC changes. Auxiliary data, in the form of a digital elevation model (DEM) with 30 m resolution, was acquired to highlight the Oued Allala watershed.

Based on very-high-resolution images, training and validation data were generated to process the classification. According to the Landsat-5 TM image resolution and study area analysis, five LULC classes were defined: built-up, forest, roads, cultivable lands, and barren lands.

3.1.2 Multi-resolution Segmentation

Because OBIA considers the spectral, textual, and contextual information of pixels, segmentation is an important step in this process. The segmentation process regroups neighboring pixels with similar characteristics. Indeed, for each image, using input spectral bands, the multi-resolution segmentation algorithm [4] was used to generate homogenous objects. Multi-resolution segmentation is a powerful algorithm designed to iteratively segment a satellite image into objects according to conditions imposed by the user [5]. In our case, using Trimble's eCognition Developer 10.0, we applied a multi-resolution algorithm to the three input images to provide segmentation layers. The identification of objects using this algorithm is built upon relative image object homogeneity or heterogeneity, based on spectral and shape criteria [12]. The size of objects is set by a scale parameter (in this study, the scale parameter = 30 for Landsat images and 10 for the Sentinel-2 image). Heterogeneity of objects is defined by shape and color parameters, in which their proportion is specified by the shape parameter (in this study, shape parameter = 0.1), which means that heterogeneity is influenced 10% by shape and 90% by color) [23, 26]. Similarly, the shape parameter is defined by two components, compactness and smoothness, in which their proportion is specified by the compactness parameter (in this study, compactness parameter = 0.9), which means that heterogeneity is influenced 90% by compactness and 10% by smoothness.

3.1.3 OBIA Classification–Based Machine Learning Classifiers

Machine learning algorithmes are widely used in remote sensing community to LULC change detection [11, 17, 33] based on multiple algorithms, namely, RF, SVM, and maximum likelihood, are widely used to detect changes in LULC. In our study, machine learning algorithms were taught the classification step through generated training samples data. Two classifiers were applied in this stage, RF and SVM. RF is a non-parametric algorithm that performs on multiple decision trees. Each decision tree is constructed using a bootstrap sample driven by different subsets. Each unique set of trees is then applied in order to classify the image, resulting in the final classification, which is a collection of multiple trees and which assigns classes by majority voting. The RF algorithm is simple to execute and only two parameters need to be set up: the number of trees and the number of features in each split. Regarding classification using the SVM algorithm, it is based on the linear function kernel. The principle of this algorithm is to find a hyperplane that separates two classes. The values closed to the hyperplane are the support vectors. The two

essential parameters of this algorithm are parameter C that controls the complexity of the classifier and parameter γ that controls the number of carrier vectors to obtain the best hyperplane [21].

3.2 LULC Map Validation

The validation of LULC maps is an indispensable step that confirms the precision of the used methods and the possibility of their use for LULC change assessments. The validation of LULC classified images was conducted through the confusion matrix using validation data. From the confusion matrix, we calculated the coefficients typically utilized in accuracy assessments, the kappa index, and the overall accuracy (OA). The producer's accuracy (PA) and user's accuracy (UA) of the LULC classes were also derived. The PA for a given LULC class shows the probability that a pixel assigned to that class in the ground data will be assigned to that class in the LULC map. The UA shows the conditional probability that a pixel classified into this class in the LULC map will be classified into this class in the ground data [35].

3.3 LULC Change Detection

Based on the three final LULC maps of 1999, 2009, and 2020, changes were assessed using the MC method implemented in Arc GIS used to generate the transition matrix of LULC classes. The MC model is a stochastic process [31, 34] that assigns the probability of the transition of land cover classes from one class to another. LULC changes for the studied area were recorded over two periods, 1999–2009 and 2009–2020. At the same time, a transition matrix was calculated for both periods using a combination of two classified images. A transition area matrix was also computed using a probability matrix. Area transition represents the total area (in cells) forecasted to change from one LULC class to another over the prescribed number of time units [33].

4 Results

4.1 Accuracy Assessment of LULC Classification

The accuracy assessment results of LULC classifications indicate high overall accuracies for both the Sentinel-2 and Landsat-5 input images. Table 1 illustrates the results of the overall accuracies (OA) and the kappa coefficient of the LULC

classified images for 1999, 2009, and 2020. As well, when the algorithms were compared, higher accuracies were obtained with the RF algorithm applied to the Sentinel-2 image (2020), with an OA of 96.6% and kappa coefficient of 0.95. In addition, LULC classification with the Landsat image (1999) also resulted in a high accuracy, with an OA of 96.2% and a kappa coefficient of 0.95. Regarding the SVM algorithm, the OA and kappa results were also relatively high, with the higher result obtained using the 2009 Landsat image, with an OA of 94.9% and kappa of 0.93.

Regarding LULC class accuracies (UA and PA) (Table 1), with respect to the 2020 LULC classification–based RF classifier, the UA and the PA of cultivable land, roads, and barren land were both high at more than 98%. However, built-up and forest were relatively poorly classified in terms of UA and PA accuracies. Moreover, for the 2009 LULC classification, built-up and forest were well classified in terms of UA (97.8% and 100%, respectively). Cultivable lands and roads had UA values of 94.6% and 92.7%, respectively. Similarly, for the 1999 LULC classification, forest, roads, and barren lands were highly classified in terms of UA, with 99.8% for both forest and roads and 99.9% for barren land.

Considering SVM classifications over the 3 years, UA values were significantly less than RF values. As well, for the 2020 LULC classification, cultivable land and roads were highly classified in terms of UA, with 90.7% and 86.8%, respectively. However, built-up and barren land were relatively poorly classified; the UA was 54% for built-up and 77% for barren land. For 1999, the LULC classification using the SVM algorithm, forest and barren lands were highly classified, with UA values of 90% for forest and 85.6% for barren land. For the 2009 LULC classification, forest and cultivable lands were well classified compared to other classes, with an UA up to 99% for both classes. Cultivable land and roads for this year stand as poorly classified, with a low UA value (up to 66%).

Overall, comparing both remote sensing data types used to produce LULC maps based on machine learning classifiers (RF and SVM), RF gives higher results, in

Table 1 Accuracy assessment of classification

Class	Metrics (%)	1999		2009		2020	
		RF	SVM	RF	SVM	RF	SVM
Built-up	UA	98.1	80.9	97.8	91	97.7	54.9
	PA	99.9	92.7	93.8	98.9	100	96.6
Forest	UA	99.8	90	100	99	97.71	81.7
	PA	92.6	86.7	92.2	99.9	100	86.8
Roads	UA	99.8	81.5	92.7	66.7	99.8	88
	PA	93.02	72.1	99.8	99.9	100	77.1
Cultivable land	UA	88.2	71.3	94.6	95.3	98	82.9
	PA	98.9	84.6	94.6	87.2	90.9	90.7
Barren land	UA	99.9	85.6	95	95.1	100	77.8
	PA	99.8	56.3	88.4	91	90	54.8
OA		96.2	81.9	94.9	94.5	96.6	76.2
Kappa		0.95	0.7	0.93	0.93	0.96	0.7

particular with Sentinel-2 data, 0.4% higher than the OA of the 1999 Landsat classification, and 1.7% higher than the OA of the 2009 Landsat classification. Regarding SVM, the higher result was obtained with the Landsat image for 2009, with a significant percentage difference of 18.3% compared to the one of 2020 and 12.6% compared to the 1999 SVM results. Between the two algorithms, regardless of the type of input image, RF outperformed SVM by 20.4% for 2020, 0.4% for 2009, and 14.3% for 1999.

4.2 Analysis of LULC Changes

The LULC classification maps for the years 1999, 2009, and 2020 are illustrated in Fig. 3. Notably, LULC has undergone considerable changes between 1999 and 2020. Additionally, according to the results of area calculations for each LULC class represented in Table 2, changes in LULC trends were observed for all LULC types.

Indeed, in 1999, the Allala watershed was dominated by cultivable land area, with a percentage of 53%, followed by barren lands (28%), forest (16.1%), built-up (1.7%), and roads (0.3%).

In 2009, considerable changes were noted in LULC trends, with the amount of land devoted to roads significantly increasing (from 0.2% to 12.2%) for the total area. Similarly, the built-up class increased remarkably (Fig. 3 and Table 2). In contrast, the barren class has undergone a significant decrease (from 28.4% to 13%) for the total area.

In 2020, there was a similar decrease for the barren land class, down to 8.7% for the total area. In parallel, roads and built-up continued to increase, and there was a slight increase in cultivable lands area (from 48.8% to 49.9%). A slight decrease also was observed in forests (from 18.4% to 14%) for the total LULC area.

Over the 3 years, cultivable lands stand as the dominant class in terms of surface area as compared to other classes. In addition, during the studied period (1999–2020), the Allala watershed saw considerable changes in LULC classes, where a decrease in some classes corresponded to an increase in others. These changes can be better explained by analyzing the LULC transition matrix.

4.3 Analysis of LULC Transition Matrix

Detailed results of the LULC transition matrices from 1999 to 2009 and 2009 to 2020 are shown in Tables 3 and 4. The analysis of the LULC transition matrices indicates significant trends in LULC transitions from one LULC type to another. According to Table 3 (1999–2009), a high transition rate was observed in the forest class, which converted into cultivable lands with 773.4 ha, cultivable lands into

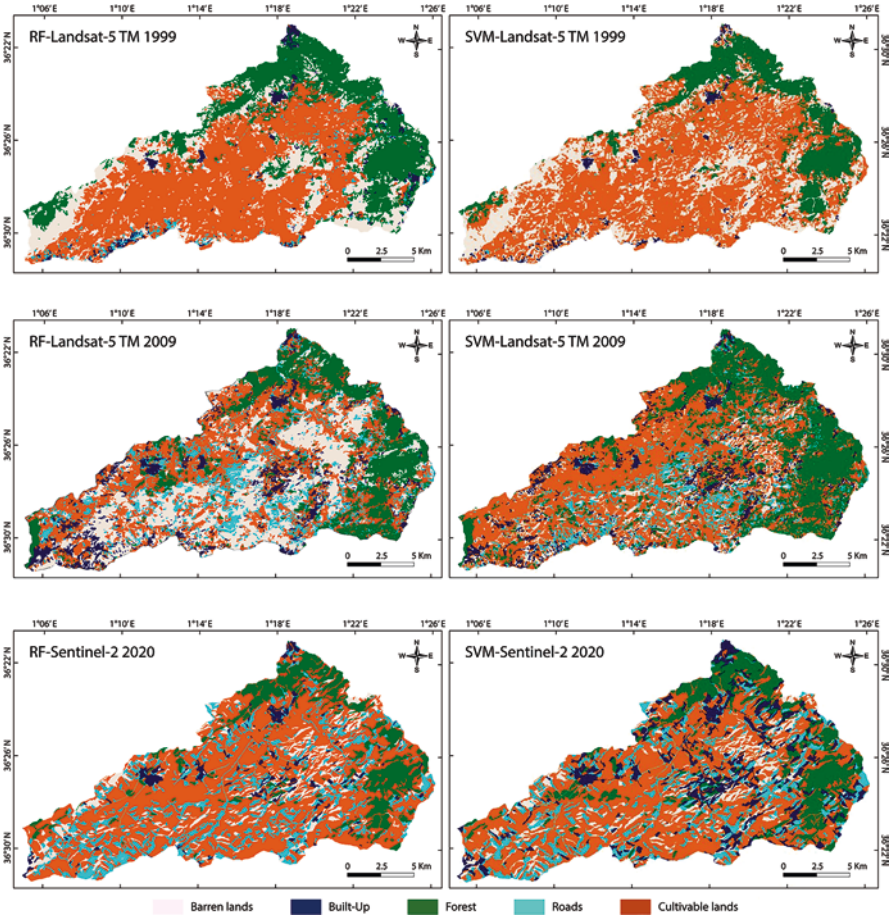

Fig. 3 LULC classification of 1999, 2009, and 2020

Table 2 LULC class areas

	1999		2009		2020	
	Area (ha)	% of total area	Area (ha)	% of total area	Area (ha)	% of total area
Built-up	537.2	1.7	2339.3	7.6	3720.1	12.1
Forest	4957.4	16.1	5652.2	18.4	4300.1	14
Roads	96.7	0.3	3736	12.2	4714.1	15.4
Cultivable land	16387.8	53.4	15,001	48.8	15307.5	49.9
Barren land	8726.6	28.4	3979	13	2664	8.7

Table 3 Transition matrix for 1999–2009 period

	LULC classes (2009) (ha)					
LULC classes (1999) (ha)	Built-up	Forest	Roads	Cultivable lands	Barren lands	Total
Built-up	359.7	15.8	30.5	34.9	92.6	533.4
Forest	14	3659	131.1	773.4	368.5	4946
Roads	7.7	7.1	10.7	27.1	43.9	96.5
Cultivable lands	373.7	1344.1	2373.7	6294.7	5989.5	16375.7
Barren lands	1577.3	611.9	1185.5	3180.7	2152.8	8708.2
Total	2332.3	5637.9	3731.6	10310.7	8647.3	30659.8

Table 4 Transition matrix for 2009–2020 period

	LULC classes 2020 (ha)					
LULC classes 2009 (ha)	Built-up	Forest	Roads	Cultivable lands	Barren land	Total
Built-up	977.5	20.3	486.7	119.0	729.8	2333.4
Forest	338.0	3186.8	176.3	1436.8	502.9	5640.8
Roads	570.9	122.6	833.3	898.0	1307.5	3732.3
Cultivable lands	1173.6	624.3	1664.9	4698.2	2153.8	10314.9
Barren land	652.9	341.7	1544.1	1896.6	4214.0	8649.3
Total	3713.0	4295.8	4705.3	9048.6	8908.0	30670.8

barren lands with 5989.5 ha, and barren lands to roads, built-up, and cultivable lands with 1185.5 ha, 1577.3 ha, and 3180.7 ha, respectively.

Regarding transitions between 2009 and 2020 (Table 4), the most significant transitions were reported for forest into cultivable lands with 1436.8 ha for the total forest area, barren land into cultivable lands with 1896.6 ha and roads with 1544.1 ha, and cultivable lands into barren lands, roads, and built-up with 2153.8 ha, 1664.9 ha, and 1173.6 ha, respectively.

5 Discussion

In this study, we aimed to map and detect LULC changes in the Allala watershed for over 21 years. Both the OBIA method based on machine learning classifiers and Arc GIS applications were used in the analysis of two Landsat images and one Sentinel-2 image. These images were gathered using remote sensing techniques and covered the years 1999, 2009, and 2020. The LULC classes in question were: built-up, forest, barren land, roads, and cultivable lands. Furthermore, in order to achieve the best possible accuracies in the change detection step, two machine learning algorithms were tested: RF and SVM. The best of both was used to detect LCLU changes.

The RF and SVM machine learning algorithms both achieved good results, with an overall accuracy ranging from 76% to 96%. In addition, the RF algorithm outperformed SVM in all LCLU classifications, regardless of the remote sensing types

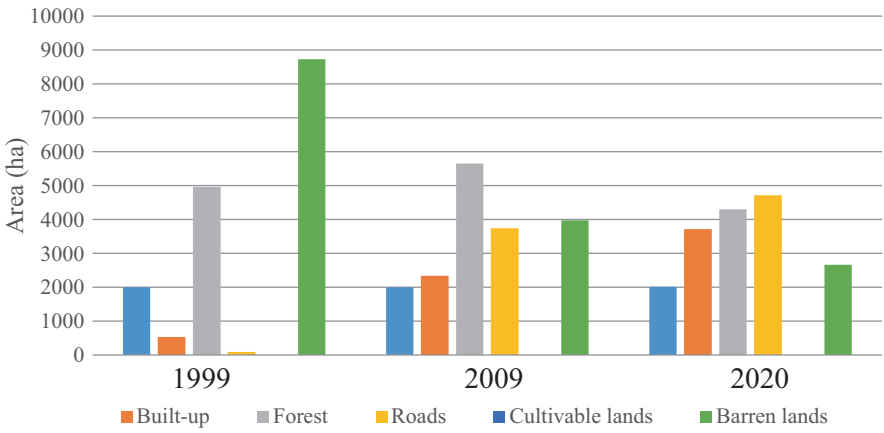

Fig. 4 Area of LULC classes of the total area (ha) over 1999, 2009, and 2020

used in the classification process. This is mentioned in several studies, for instance, [3, 15, 19, 38]. In our case, the optimization of parameters of the used classifiers has allowed us to obtain better results with high values of the overall accuracy.

Additionally, our experiments exhibited that RF performed better on the Sentinel-2 image than on the Landsat images and gives the highest value of the overall accuracy (up to 96%). These results confirm the efficacy and robustness of this algorithm when applied to this type of data, particularly for LULC mapping [39, 40]. In addition, this is strongly explained by the spatial resolution effect.

By UA and PA calculations (Table 1), the accuracy of the classes has also been evaluated within each algorithm for the 3 years. As well, for 1999 and 2020, built-up and barren land were well detected with RF, with UA and PA values at more than 96%. For 2009, forest was well classified with an UA and a PA of more than 92%. However, the worst class in terms of UA and PA was barren lands with values close to 54%. However, despite the high values of the overall precision of some classes especially roads. This class was not well delineated and took up a large area compared to other classes. This is due to the effect of the segmentation of the satellite image and in particular the "scale" parameter which generated large segments which then affected the final classification.

Considering the results of LULC change detection over the two periods, 1999–2009 and 2009–2020, as observed from the final LULC maps (Fig. 3), in addition to the results shown in Table 2 and Fig. 4, the Allala watershed has undergone different change trends over the studied years. Additionally, according to transition matrix results over 1999–2009 and 2009–2020 (Tables 3 and 4), the LULC is progressively transitioning from one LULC class to another.

Obviously, a great increase in area of both built-up and roads is observed, which is explained by the population growth and subsequent urbanization. This also facilitated the transition of some classes to built-up and roads. This increase was offset by a big decrease in the barren land class, 15.4% from 1999 to 2009 and 4.3% from

2009 to 2020. Specifically, the change rate is more significant during the 1999–2009 period. These results are logical, as Ténès City has been under constant urban construction over the last decades.

As well, the forest class has decreased by 2.1% from 1999 to 2020. This is explained by the degradation of watershed ecosystems and the many forest fires this region has experienced. Furthermore, the cultivable land class, which occupies the largest proportion of the total watershed area (53.4% in 1999), has decreased by 4.6% from 1999 to 2009 and then increased by 1.1% from 2009 to 2020. This is generally related to the harvest season when satellite images were acquired.

Moreover, forest area has been converted into barren land (7.7%) and cultivable land (15.6%). Regarding transitions between 2009 and 2020, the most important transitions were reported for forest into cultivable lands (16%) and barren land into built-up (18%), roads (14%), and cultivable lands (37%). This is explained by the forest degradation in the Allala watershed.

6 Conclusion

This study mapped and assessed land use and land cover changes in the Oued Allala watershed for over 21 years. The OBIA approach applied on two Landsat-5 TM images, taken in 1999 and 2009, and one Sentinel-2 image from 2020 enabled the identification of the changes in LULC and the distribution of area classes in the total watershed area for over 21 years. Consequently, machine learning classifiers applied with OBIA obtained higher accuracies of LULC classification (>90% overall accuracy). Specifically, the RF machine learning classifier outperformed SVM with all data over the 3 years (> 96%). In addition, the proposed methodology combined remote sensing results with Geographic Information System (GIS) tools in order to assess LULC changes efficiently.

According to the results of LULC change detection, Oued Allala has undergone many changes over time. These results confirm that the region has undergone many environmental changes in recent decades due to the growth in population, urbanization, and the evolution of agricultural areas. Notable changes include an increase in building (15.4%), cultivable land (1.1%), and road (10.9%) classes and a decrease in forests (4.4%) and barren land (4.3%). Hence, the change rate is more significant in the 1999–2009 period. These statistics are logical, as Ténès City was still under urban construction during this period. However, analyzing the transition matrix results showed that the most significant transitions were reported for forest into cultivable lands (16%), which is confirmed by the deforestation in the region. Barren land also transited into built-up (18%), roads (14%), and cultivable lands (37%).

Analyzing and mapping the trends of LULC changes in the studied area provide a basis for strategic planning, managing, and protection decision-making, and the results of LULC change analysis can be used as a decision support tool and further help in regional and national land management.

Acknowledgments This research was funded by the Hubert Curien PHC-Tassili project (19 MDU 207), the interdisciplinary graduate school for the blue planet (ISblue), and the program of ERASMUS + Chair Jean Monnet European Spatial Studies of Sea and Coastal zones – 599967-EPP-1-2018-1-FR-EPPJMO-CHAIR.

References

1. Abdullah AYM et al (2019) Spatio-temporal patterns of land use/land cover change in the heterogeneous coastal region of Bangladesh between 1990 and 2017. Remote Sens 11:790
2. Adafer S, Bensaibi M (2017) Seismic vulnerability classification of roads. Energy Procedia 139:624–630
3. Adugna T, Xu W, Fan J (2022) Comparison of random forest and support vector machine classifiers for regional land cover mapping using coarse resolution FY-3C images. Remote Sens 14:574
4. Baatz M, Schäpe A (2000) Multiresolution Segmentation: an optimization approach for high quality multi-scale image segmentation. Proceedings of Angewandte Geographische Informationsverarbeitung XII, p 12
5. Belgiu M, Csillik O (2018) Sentinel-2 cropland mapping using pixel-based and object-based time-weighted dynamic time warping analysis. Remote Sens Environ 204:509–523
6. Bello OM, Aina YA (2014) Satellite remote sensing as a tool in disaster management and sustainable development: towards a synergistic approach. Procedia Soc Behav Sci 120:365–373
7. Bentekhici N (2020) Contribution of remote sensing and GIS to mapping the fire risk of Mediterranean forest case of the forest massif of Tlemcen (North-West Algeria). Nat Hazards 21
8. Blaschke T (2010) Object based image analysis for remote sensing. ISPRS J Photogramm Remote Sens 65:2–16
9. Castillejo-González IL et al (2009) Object- and pixel-based analysis for mapping crops and their agro-environmental associated measures using QuickBird imagery. Comput Electron Agric 68:207–215
10. Chen G, Hay GJ, Carvalho LMT, Wulder MA (2012) Object-based change detection. Int J Remote Sens 33:4434–4457
11. Chen Y, Ming D, Lv X (2019) Superpixel based land cover classification of VHR satellite image combining multi-scale CNN and scale parameter estimation. Earth Sci Inform 12:341–363
12. eCognition (2021) [En ligne]. Disponible sur: https://fr.geospatial.trimble.com/products-and-solutions/ecognition
13. Farjad B, Gupta A, Razavi S, Faramarzi M, Marceau D (2017) An integrated modelling system to predict hydrological processes under climate and land-use/cover change scenarios. Water 9:767
14. Garg V et al (2019) Human-induced land use land cover change and its impact on hydrology. Hydro Res 1:48–56
15. Ghosh A, Joshi PK (2014) A comparison of selected classification algorithms for mapping bamboo patches in lower Gangetic plains using very high resolution WorldView 2 imagery. Int J Appl Earth Obs Geoinf 26:298–311
16. Guan D et al (2011) Modeling urban land use change by the integration of cellular automaton and Markov model. Ecol Model 222:3761–3772
17. Halmy MWA, Gessler PE, Hicke JA, Salem BB (2015) Land use/land cover change detection and prediction in the north-western coastal desert of Egypt using Markov-CA. Appl Geogr 63:101–112
18. Hansen MC, Defries RS, Townshend JRG, Sohlberg R (2000) Global land cover classification at 1 km spatial resolution using a classification tree approach. Int J Remote Sens 21:1331–1364

19. Htitiou A et al (2019) The performance of random forest classification based on phenological metrics derived from Sentinel-2 and Landsat 8 to map crop cover in an irrigated semi-arid region. Remote Sens Earth Syst Sci 2:208–224
20. How Jin Aik D, Ismail MH, Muharam FM (2020) Land use/land cover changes and the relationship with land surface temperature using landsat and MODIS imageries in Cameron Highlands, Malaysia. Land 9:372
21. Huang C, Davis LS, Townshend JRG (2002) An assessment of support vector machines for land cover classification. Int J Remote Sens 23:725–749
22. Kastali A et al (2021) Design flood and flood-prone areas under rating curve uncertainty: area of Vieux-Ténès. Algeria J Hydrol Eng 26:1–12
23. Lourenço P et al (2021) Assessing the performance of different OBIA software approaches for mapping invasive alien plants along roads with remote sensing data. Int J Appl Earth Obs Geoinf 95:102263
24. Mas J-F (1999) Monitoring land-cover changes: a comparison of change detection techniques. Int J Remote Sens 20:139–152
25. Myint SW, Gober P, Brazel A, Grossman-Clarke S, Weng Q (2011) Per-pixel vs. object-based classification of urban land cover extraction using high spatial resolution imagery. Remote Sens Environ 115:1145–1161
26. Platt RV, Ogra MV, Badola R, Hussain SA (2016) Conservation-induced resettlement as a driver of land cover change in India: an object-based trend analysis. Appl Geogr 69:75–86
27. Psomiadis E, Soulis K, Zoka M, Dercas N (2019) Synergistic approach of remote sensing and GIS techniques for flash-flood monitoring and damage assessment in Thessaly Plain Area, Greece. Water 11:448
28. Putri LM, Wicaksono P (2021) Mapping of land use changes in the core zone of parangtritis sand dunes using OBIA method 2015–2020. JG 13:109
29. Sehili F, Madani S (2017) The policies of seismic risk management: case of the protected areas of Dellys and Tenes Cities, Algeria. Int J Civ Eng 11
30. Singh A (1989) Review Article Digital change detection techniques using remotely-sensed data. Int J Remote Sens 10:989–1003
31. Sinha P, Kumar L (2013) Markov land cover change modeling using pairs of time-series satellite images. Photogramm Eng Remote Sens 79:1037–1051
32. Veldkamp A, Lambin EF (2001) Predicting land-use change. Agric Ecosyst Environ 85:1–6
33. Wang SW, Gebru BM, Lamchin M, Kayastha RB, Lee W-K (2020) Land use and land cover change detection and prediction in the Kathmandu District of Nepal using remote sensing and GIS. Sustainability 12:3925
34. Weng Q (2002) Land use change analysis in the Zhujiang Delta of China using satellite remote sensing, GIS and stochastic modelling. J Environ Manage 64:273–284
35. Yan G, Mas J-F, Maathuis BHP, Xiangmin Z, Van Dijk PM (2006) Comparison of pixel-based and object-oriented image classification approaches—a case study in a coal fire area, Wuda, Inner Mongolia. China Int J Remote Sens 27:4039–4055
36. Yin J, He F, Xiong YJ, Qiu GY (2017) Effects of land use/land cover and climate changes on surface runoff in a semi-humid and semi-arid transition zone in Northwest China. Hydrol Earth Syst Sci 21:183–196
37. Zaabar N, Niculescu S, Mihoubi MK (2021) Assessment of combining convolutional neural networks and object based image analysis to land cover classification using Sentinel 2 satellite imagery (Tenes region, Algeria). Int Arch Photogramm Remote Sens Spatial Inf Sci XLIII-B3-2021:383–389
38. Zaabar N, Niculescu S, Mihoubi MK (2022) Application of convolutional neural networks with object-based image analysis for land cover and land use mapping in coastal areas: a case study in Ain Témouchent, Algeria. IEEE J Sel Top Appl Earth Obs Remote Sens:1–16. https://doi.org/10.1109/JSTARS.2022.3185185

39. Zeroual A, Assani AA, Meddi M (2017) Combined analysis of temperature and rainfall variability as they relate to climate indices in Northern Algeria over the 1972–2013 period. Hydrol Res 12
40. Zope PE, Eldho TI, Jothiprakash V (2017) Hydrological impacts of land use–land cover change and detention basins on urban flood hazard: a case study of Poisar River basin, Mumbai, India. Nat Hazards 87:1267–1283